Lignin as a multifunctional photocatalyst for solar-powered biocatalytic oxyfunctionalization of C-H bonds

Jinhyun Kim,[a] Frank Hollmann,[b] and Chan Beum Park*[a]

[a] Department of Materials Science and Engineering, Korea Advanced Institute of Science and Technology (KAIST), 335 Science Road, Daejeon 305-701, Republic of Korea;
[b] Department of Biotechnology, Delft University of Technology, Van der Maasweg 9, 2629HZ Delft, The Netherlands. *E-mail: parkcb@kaist.ac.kr

Abstract

Lignin is a key structural material in all terrestrial plants that is responsible for cell wall formation, water transportation, seed protection, and stress adaptation. Each year, pulp and paper industry produces approximately 50 million metric tons of lignin as waste, 95% of which is combusted or abandoned. Here, we report a new multifunctionality of lignin as a photocatalyst (e.g., synergistic formation of H_2O_2 formation through O_2 reduction and H_2O oxidation, use of H_2O as an electron donor, and $OH^{\bullet}$-scavenging activity). Our spectroscopic and photoelectrochemical analyses reveal the photophysical characteristics (e.g., light absorption, charge separation/transfer) of lignin models [e.g., lignosulfonate (LS) and kraft lignin (KL)] and their electronic properties [HOMO-LUMO gap: 2.67 eV (LS), 2.95 eV (KL), LUMO: -0.23 V_{RHE} (LS) and -0.26 V_{RHE} (KL), HOMO: 2.44 V_{RHE} (LS) and 2.69 V_{RHE} (KL)]. We demonstrate lignin-sensitized redox chemistry, such as (i) H_2O_2 formation through O_2 reduction using H_2O as an electron donor and (ii) O_2 evolution through H_2O oxidation, under visible light. Furthermore, the integration of lignin and H_2O_2-dependent unspecific peroxygenases (UPOs) enables enantiospecific oxyfunctionalization reactions (e.g., benzylic hydroxylation, alkane hydroxylation, styrene epoxidation). Lignin photocatalysts solve existing issues (e.g., requirement of artificial electron donors, H_2O_2- or $OH^{\bullet}$-driven inactivation of UPO) related to the sustainable activation of UPO. The lignin/UPO hybrid achieves a total turnover number of enzyme of 81070, the highest value ever recorded for solar-powered biocatalytic

oxyfunctionalization in photochemical platforms. This work demonstrates the propriety of lignin in robust photocatalyst/biocatalyst hybrids for artificial photosynthesis.

Keywords: lignin, photobiocatalysis, artificial photosynthesis, redox biocatalysis, selective oxyfunctionalization

Introduction

Selective oxyfunctionalization reactions of nonactivated C-H bonds are the holy grail in synthetic chemistry because they require the reorganization of kinetically inert C-H bonds.[1] Heme-thiolate enzymes have garnered much interest because of their high reactivity, selectivity, and a broad substrate range.[2,3] Nowadays, cytochrome P450 monooxygenases are used widely as biocatalysts[4] to oxyfunctionalize hydrocarbons, but they depend on complex electron transport pathways,[5] requiring one molecular oxygen and two electrons that are delivered by redox equivalents [e.g., 1,4-dihydronicotinamide adenine dinucleotide or its phosphorylated form, NAD(P)H]. In contrast, unspecific peroxygenases (UPOs, IUBMB classification: EC 1.11.2.1) use hydrogen peroxide (H_2O_2) only to generate the catalytically active oxoferryl-heme (Compound I) through the peroxide shunt pathway,[3,5] making UPOs a promising alternative to P450 monooxygenases and chemical counterparts.

Nevertheless, UPOs suffer from the oxidative inactivation of their heme active sites in the presence of elevated concentrations of H_2O_2.[6] This instability has been addressed through the use of additional redox catalysts[3,4,7,8] that facilitate *in situ* H_2O_2 supply in adequate concentrations. Most of these catalysts reduce O_2 to H_2O_2 ($O_2 + 2H^+ + 2e^- \rightarrow H_2O_2$) at the expense of artificial electron donors (e.g., alcohol[4], formate[7,8]) or cosubstrates (e.g., glucose[3]). This necessity complicates the reaction schemes and causes serious issues, such as poor atom economy (e.g., 16.03% for the glucose/glucose oxidase systems[3]) and the accumulation of undesirable side products (e.g., gluconic acid[4,9]). The challenge can be circumvented if the redox catalyst can use water as an electron donor and a cosubstrate in O_2 reduction to H_2O_2 and H_2O oxidation to H_2O_2, respectively. This strategy is based on (i) water's role as a solvent in UPO catalysis, (ii) its abundance (55.55 M), (iii) the near-unity atom economy of H_2O_2 production (94.44%; $2H_2O \rightarrow H_2O_2 + 2H^+ + 2e^-$), and (iv) O_2 molecules as a side product of

water oxidation ($2H_2O \rightarrow O_2 + 4H^+ + 4e^-$)[10]. Despite these merits, water oxidation catalysts have the disadvantage of producing reactive oxygen species, which is detrimental to UPO-driven catalysis. For example, cutting-edge photochemical systems[8,9,11] oxidize H_2O to hydroxyl radicals ($OH^\bullet$) that inactivate UPOs.

Here, we report lignin as a multifunctional photocatalyst that accomplishes such challenging goals (i.e., *in situ* H_2O_2 formation through O_2 reduction and H_2O oxidation, use of H_2O as an electron donor, and $OH^\bullet$-scavenging activity) for sustainable UPO catalysis under visible light (**Fig. 1**). Solar energy holds great promise as an abundant, sustainable, and clean resource of chemical potential[12-15]; hence, photocatalysts have been applied extensively for solar-to-chemical conversion (e.g., aliphatics production[16,17], hydrogen evolution[18,19], methanation[20]). Lignin—the second most earth-abundant biopolymer—is highly functionalized with various aromatic unit structures in lignocellulosic biomass.[21,22] The pulp, paper, and biofuel industries generate lignin as waste with an annual production of around 50 million metric tons.[23] However, 95% of lignin is abandoned or combusted[23,24] in biorefinery processes because of its complex, irregular, and ill-defined chemical structure.[21,23,25] Recently, lignin materials have been studied to (i) prepare value-added aromatics[26] and (ii) use themselves as building blocks[21] for energy and environmental applications.

Moving beyond these conventional approaches, we hypothesize that lignin polymers can perform photoredox reactions because they contain π-conjugated systems with redox moieties that most molecular photocatalysts share[27,28]; delocalized electrons in circular π bonds can be photoexcited to energetically higher levels, causing them to participate in photoinduced electron transfer for solar-driven redox chemistry. Inspired by their molecular structures, we investigate lignin's electronic and photophysical properties and demonstrate lignin-sensitized H_2O_2 formation (through O_2 reduction and H_2O oxidation) and O_2 evolution (through H_2O oxidation) under visible light. This synergistic photoredox reaction is further combined with

peroxygenase biocatalysis to accomplish the photoenzymatic oxidation of nonactivated C-H bonds and thus synthesize enantiopure alcohols and epoxides [i.e., enantiomeric excess (*ee*) > 99%]. Furthermore, the lignin photocatalysts function as an antioxidant to suppress $OH^{\bullet}$-mediated UPO inactivation. This enables the lignin/peroxygenase system to achieve the highest-ever-recorded longest reaction time and total turnover number of 130 h and 81070, respectively, among solar-assisted biocatalytic oxyfunctionalization studies.

Results

Electronic and photophysical properties of lignins

We chose lignosulfonate (LS) and kraft lignin (KL) as our model lignin. These lignin macromolecules are isolated from lignocellulosic biomass via sulfite and kraft pulping processes, respectively.[21] The different chemical treatments give LS and KL rather different chemical and redox properties. To better understand the origin of lignin's photocatalytic activity, we investigated the optical absorption property using ultraviolet-visible (UV-Vis) spectroscopy. KL exhibited a stronger photoabsorption from UV to visible light region compared with LS (**Supplementary Fig. 1a**). The energy gaps between the LS and KL's highest occupied molecular orbital (HOMO) and the lowest unoccupied molecular orbital (LUMO) were estimated to be *ca.* 2.67 and 2.95 eV, respectively, based on the absorption analysis (**Supplementary Figs. 1b and 1c**). Next, we used ultraviolet photoelectron spectroscopy to estimate the HOMO levels of the lignins. Note that the photoemission spectroscopy is used widely to characterize the valence electronic states of organic materials.[29] We found that LS and KL's HOMO levels were 2.44 and 2.69 V (vs. reversible hydrogen electrode, RHE), respectively (**Supplementary Fig. 2**). Thus, the LUMO energies of LS and

KL were calculated to be -0.23 and -0.26 V_{RHE}, respectively, based on their HOMO-LUMO gaps (**Fig. 2a**).

The separation/recombination and transfer of photoexcited charge carriers are key factors in photoredox reactions because the charge carriers must be delivered to adjacent substrates. We found that KL exhibited more efficient charge separation than LS; according to the photoluminescence spectra of LS and KL (**Supplementary Fig. 3**), the emission intensity of KL was much lower than that of LS, which we attribute to slower charge recombination in KL. Furthermore, KL exhibited better charge transfer ability than LS. According to our chopped-light chronoamperometric analysis (**Fig. 2b**), the photocurrent of KL was approximately four times higher than that of LS under visible light (λ > 400 nm). This photosensitization results from their HOMO-LUMO gaps in the visible range (**Fig. 2a and Supplementary Figs. 1b and 1c**). The difference in the lignins' charge transport properties were further supported by electrochemical impedance spectroscopic analysis; we measured the charge transfer resistance of lignins using Nyquist plots, which were fitted to the Randles circuit model. As shown in **Fig. 2c**, KL exhibited lower charge-transfer resistance than LS under visible light. Furthermore, LS and KL were highly stable under visible light (**Supplementary Fig. 4**), which contrasts with the rapid photobleaching of many common photocatalysts.[7,10]

Lignin-sensitized reduction of O_2 to H_2O_2 under visible light

Building on the electronic and photophysical properties of lignins, we investigated their capability to photocatalytically reduce O_2 to H_2O_2 because the reduction potential of O_2/H_2O_2 [**equation (1)**][30] is more positive than the lignins' LUMO levels (**Fig. 2a**).

$$O_2\,(aq) + 2\,(H^+ + e^-) \rightarrow H_2O_2\,(aq),\ E_{red} = 1.14\ V_{RHE} \qquad (1)$$

In addition to the thermodynamic requirement, the interaction between the electron acceptor (e.g., dioxygen) and the donor (e.g., lignins) plays an important role in redox catalysis. Thus, we used UV-Vis spectroscopy to examine the attractive interaction between O_2 and the π-conjugated moieties of lignins. As shown in **Supplementary Fig. 5**, the absorbance of LS and KL gradually increased with the O_2 purging time. This result indicates that lone pair-π interactions change π-π* electronic transitions[31] of π-functionalities (e.g., phenoxy groups, conjugated carbonyl groups) in lignin's monomeric phenylpropanes.

Having substantiated the favorable noncovalent interaction between the lignins and O_2, we exposed a lignin solution (1 mg mL^{-1}) in an O_2-enriched phosphate buffer (KPi, 100 mM, pH 7.0) to visible light from a solar simulator ($\lambda > 400$ nm). Photoactivated LS and KL gradually accumulated H_2O_2 at a rate of 79.92 ± 19.35 and 158.49 ± 25.13 mM g_{cat}^{-1} h^{-1}, respectively (**Fig. 3a**). We attribute KL's faster H_2O_2 production to its higher light absorption, charge separation, and charge transfer (**Supplementary Figs. 1a and 3 and Figs. 2b and 2c**). When we irradiated the lignin solutions with monochromated light, the apparent quantum yields of LS and KL decreased with the increasing wavelength of the incident light (**Supplementary Fig. 6**); these action spectra of LS and KL were analogous to the lignins' absorption spectra, indicating that photoactivation of LS and KL is the key step for H_2O_2 formation. Control experiments in the absence of lignins or light resulted in a negligible H_2O_2 production (**Fig. 3a and Supplementary Fig. 7**).

The reduction of O_2 to H_2O_2 can proceed through (i) a two-step, single-electron reduction (i.e., $O_2 \rightarrow O_2^{\bullet-} \rightarrow H_2O_2$) or (ii) a one-step, two-electron reduction (i.e., $O_2 \rightarrow H_2O_2$) route.[32] To elucidate the pathway of lignin-sensitized H_2O_2 production, we analyzed the formation of superoxide ions ($O_2^{\bullet-}$) using a nitroblue tetrazolium assay[10] (**Supplementary Fig. 8a**). LS and KL photocatalysts produced $O_2^{\bullet-}$ under visible light in an O_2-enriched environment, whereas a negligible amount of the ion was detected under N_2-rich or dark

conditions (**Supplementary Fig. 8b**). The addition of 1,4-benzoquinone ($O_2^{\bullet-}$ scavenger)[33] into an O_2-purged lignin solution decreased the rate of H_2O_2 formation by LS and KL photocatalysts (**Fig. 3b, left panel**), which supports the two-step reduction of O_2 to H_2O_2.

Photocatalytic H_2O oxidation to H_2O_2 and O_2

We paid particular attention to the absence of artificial electron donors for the lignin-catalyzed production of H_2O_2 because the incomplete depression of H_2O_2 formation (**Fig. 3b, left panel**) can originate from the oxidation of the H_2O solvent to H_2O_2. This motivated us to evaluate the capability of photoactive lignins to oxidize H_2O. Note that lignin photoexcitation enables thermodynamically favorable oxidation of H_2O to H_2O_2 [**equation (2)**][10] because the HOMO levels of LS and KL are more positive than the oxidation potential of H_2O to H_2O_2 (**Fig. 2a**).

$$2H_2O\ (l) \rightarrow H_2O_2\ (aq) + 2\ (H^+ + e^-),\ E_{ox} = 1.76\ V_{RHE} \qquad (2)$$

To exclude H_2O_2 production *via* O_2 reduction reaction, we purged N_2 gas into a lignin solution before and during photocatalysis. As shown in **Fig. 3b (right panel)**, the rate of H_2O_2 formation decreased to 24.93 and 66.44 mM $g_{cat}^{-1}\ h^{-1}$ for LS and KL, respectively. This result indicates that water oxidation is another photocatalytic pathway for H_2O_2 production on LS and KL. The rates were almost identical to those observed in the presence of 1,4-benzoquinone ($O_2^{\bullet-}$ scavenger) under O_2-enriched conditions (**Fig. 3b, left panel**; statistically insignificant difference according to one-way analysis of variance), which implies that one-step reduction of O_2 to H_2O_2 rarely occurs. Furthermore, we also confirmed the lignin-catalyzed formation of O_2 [**equation (3)**[10] and **Supplementary Fig. 9**] using head-space gas chromatography.

$$2H_2O\ (l) \rightarrow O_2\ (g) + 4\ (H^+ + e^-),\ E_{ox} = 1.23\ V_{RHE} \qquad (3)$$

O_2 formation is thermodynamically favorable because $E_{ox}(O_2/H_2O)$ is less positive than the HOMO levels of LS and KL. Taken together, the lignin photocatalysts serve two functions: (i) the reduction of O_2 to H_2O_2 and (ii) the oxidation of H_2O to H_2O_2 and O_2.

Based on the extensively accepted mechanism of photoredox catalysis,[27,34] we propose that a possible process for O_2 reduction and H_2O oxidation using lignins involve a combination of reductive and oxidative quenching cycles of lignin photocatalysts, as depicted in **Fig. 3c**. Light absorption of lignin causes it to become a photoactivated state, $[\text{lignin}]^*$, which is both a stronger oxidant and a stronger reductant than its corresponding ground state. In a reductive quenching pathway, $[\text{lignin}]^*$ oxidizes H_2O to H_2O_2 or O_2 and becomes the reduced catalyst, $[\text{lignin}]^{\bullet-}$. This state reduces O_2 to H_2O_2 and returns to its original state. In an oxidative quenching process, the oxidized catalyst, $[\text{lignin}]^{\bullet+}$, is formed through O_2 reduction, which then reverts to its original state *via* H_2O oxidation. The HOMO and LUMO levels of LS and KL make $[\text{LS}]^*$ and $[\text{KL}]^*$ thermodynamically favorable for the photocatalytic production of H_2O_2 and O_2 through O_2 reduction and H_2O oxidation.

Enantioselective photoenzymatic oxyfunctionalization reactions

Having substantiated *in situ* H_2O_2 generation by the lignin photocatalysts, we established photobiocatalytic oxyfunctionalization reaction by coupling lignin-driven photocatalysis with peroxygenase-mediated biocatalysis in a one-pot process. We chose the UPO from *Agrocybe aegerita*, which was expressed recombinantly in *Pichia pastoris* (r*Aae*UPO)[3] because of its versatility[33] and high activity toward inert C-H bonds[35]. We tested ethylbenzene as a model substrate because the hydroxylation of a methylene C-H bond adjacent to oxidatively more labile π-functionality is very challenging[36]. As shown in **Supplementary Fig. 10**, LS/r*Aae*UPO and KL/r*Aae*UPO systems converted ethylbenzene to (*R*)-1-phenylethanol enantiospecifically

(> 99% *ee*) under visible light (λ > 400 nm). Noteworthy, the stereo- and chemoselectivity of the overall reaction was very high, in contrast to previous photoenzymatic reactions[3,4,8]; the previous studies reported the non-enzymatic oxidation of the substrate and the alcohol product to a racemic product and overoxidation product acetophenone, respectively. The omission of lignin, light, or substrate led to a negligible yield of 1-phenylethanol (**Supplementary Fig. 10**) because of the imperceptible formation of H_2O_2 under the depleted conditions (**Fig. 3a and Supplementary Fig. 7**). However, the photobiocatalytic reaction occurred under O_2-depleted conditions because of the *in situ* H_2O oxidation to H_2O_2 (**Fig. 3b and Supplementary Fig. 10**).

We investigated the kinetics of the photoenzymatic reaction with respect to lignin concentration and photon flux. As shown in **Supplementary Fig. 11a**, the turnover frequencies of r*Aae*UPO ($TOF_{rAaeUPO}$) were saturated with lignin concentration at over 8 mg mL^{-1}, indicating that H_2O_2 formation is a rate-limiting step. When we varied photon flux at a fixed lignin concentration (8 mg mL^{-1}), the $TOF_{rAaeUPO}$ of LS/r*Aae*UPO became larger than that of KL/r*Aae*UPO at over 1.16 μE cm^{-2} s^{-1} (**Supplementary Fig. 11b**). We attribute the result to the higher optical transparency of LS compared with KL (**Supplementary Fig. 12**); the self-shading effect of KL decreased light penetration, making some KL photocatalysts inactive in a reaction solution. The hydroxylation reaction exhibited a saturated $TOF_{rAaeUPO}$ at over 1.74 μE cm^{-2} s^{-1}.

We further conducted a long-term photobiocatalytic oxyfunctionalization reaction using 8 mg mL^{-1} lignin photocatalysts, 50 nM r*Aae*UPO, and 1.74 μE cm^{-2} s^{-1} visible light. The LS/r*Aae*UPO and KL/r*Aae*UPO hybrids produced enantiopure products for at least 130 h (**Supplementary Fig. 13**), thereby recording total turnover numbers of r*Aae*UPO ($TTN_{rAaeUPO}$) of 81070 and 72552, respectively (**Table 1, entry 1**). Furthermore, the lignin/r*Aae*UPO couples exhibited applicability to other enantiospecific oxyfunctionalization reactions; as summarized in **Table 1**, the light-driven enzymatic systems achieved (i) the hydroxylation of

propylbenzene, tetralin, and cyclohexane (**entries 2-4**) and (ii) the epoxidation of *cis-β*-methylstyrene (**entry 5**).

The robustness of the lignin/r*Aae*UPO hybrids is much better than those of other water oxidation catalysts/UPO systems[8,9,11]; these reported abiotic catalysts generate hydroxyl radicals to oxidatively inactivate UPOs, thus ceasing their biocatalytic reactions within 35 h. Thus, we hypothesized that water-oxidizing LS and KL energy materials do not produce hydroxyl radicals. We analyzed the formation of $OH^{\bullet}$ using a terephthalic acid assay[37]. Photoactivated LS and KL produced a negligible amount of the radical under visible light (**Supplementary Fig. 14**) although they exhibit thermodynamic favorability of $OH^{\bullet}$ formation *via* two pathways [i.e., H_2O oxidation (**equation (4)**) and H_2O_2 reduction[9] (**equation (5)**)].

$$H_2O\ (l) \rightarrow OH^{\bullet}\ (aq) + (H^+ + e^-),\ E_{ox} = 2.38\ V_{RHE} \quad (4)$$

$$H_2O_2\ (aq) + e^- \rightarrow OH^{\bullet}\ (aq) + OH^-,\ E_{red} = 0.79\ V_{RHE} \quad (5)$$

This result motivated us to investigate the $OH^{\bullet}$-scavenging activities of lignin photocatalysts. We produced hydroxyl radicals using a nanostructured hematite electrode (α-Fe_2O_3; **Supplementary Fig. 15**) and detected the radicals in the absence and presence of photoactivated lignins. As shown in **Supplementary Fig. 16**, the α-Fe_2O_3 photoanode formed $OH^{\bullet}$ radicals in an O_2-purged KPi buffer at 0.622 V_{RHE} (0 $V_{Ag/AgCl}$) under visible light (see the detailed explanations in the figure legend). In contrast, the radical was not detected when lignin photocatalysts were extant in the buffer, which indicates the antioxidant properties of lignin materials.

Discussion and Conclusion

The present work identifies the capability of lignin as a non-metallic photocatalyst. Through spectroscopic and photoelectrochemical analyses, we substantiated that LS and KL absorb visible light [HOMO-LUMO gap (in eV): 2.67 (LS) and 2.95 (KL)] to promote electronic transition to energetically higher levels [HOMO (in V_{RHE}): 2.44 (LS) and 2.69 (KL), LUMO (V_{RHE}): -0.23 (LS) and -0.26 (KL)]. Based on these thermodynamic indices of lignin photocatalysts, we unveiled lignin-sensitized (i) O_2 reduction to H_2O_2 and (ii) H_2O oxidation to H_2O_2 and O_2 under solar irradiation ($\lambda > 400$ nm). H_2O is the most desirable electron donor in aqueous redox chemistry because it is abundant and biocompatible, and simplifies reaction schemes; the thermodynamic favorability of lignin photocatalysts for H_2O oxidation makes them distinct from many other photocatalysts[7,8,32] that rely on artificial electron suppliers (e.g., formic acid, primary/secondary alcohol). In addition, lignin oxidizes H_2O to H_2O_2 and O_2; this builds up local concentrations of oxygen in the vicinity of lignin photocatalysts, which can escalate the rate of O_2 reduction to H_2O_2. The dual production of H_2O_2 and O_2 *via* the H_2O oxidation route is demonstrated for the first time in the field of photocatalysis.

Furthermore, this study reports UPO-catalyzed enantioselective oxyfunctionalization reactions (e.g., benzylic hydroxylation, alkane hydroxylation, styrene epoxidation) through lignin-driven generation of H_2O_2 *in situ* under visible light. Among photoenzymatic systems[3,8] using visible light and H_2O, lignin/UPO hybrids are more apposite in the production of enantiopure alcohols and epoxides (i.e., >99% *ee*). Furthermore, lignin's phenol-based monomeric units exhibit an antioxidative function,[21,38] which addresses the inactivation issue of UPOs against $OH^{\bullet}$ radicals; this property is a departure from $OH^{\bullet}$-generating behaviors of water oxidation catalysts[8,9,11] that halt UPO-mediated biotransformations. Thus, lignin/UPO combinations compare favorably with cutting-edge photoenzymatic systems that use r*Aae*UPO

under visible light (**Fig. 4**). Photoactive nanomaterials[3,4,8] and π-conjugated acridine derivatives[7] (e.g., gold-loaded TiO_2, graphitic C_3N_4, methylene blue, phenosafranine, flavin mononucleotide) require artificial electron donors (e.g., methanol, formate, *in situ* regenerated NADH) to achieve meaningful TTNs (10879 to 71000). The $TTN_{rAaeUPO}$ of lignin photocatalysts was the highest even at the expense of H_2O as a clean and desirable electron donor. Furthermore, the catalytic performance (e.g., *ee*, catalytic turnover) of r*Aae*UPO outweighs those of chemical catalysts and well-established P450 monooxygenases (**Supplementary Table 2**). Future challenges to enhancing enzymatic productivity would be (i) the design of a biphasic aqueous/organic system to increase the concentration of hydrophobic substrates and (ii) the conjugation of lignin with redox mediators to boost H_2O_2 formation based on energy level matching.

In conclusion, the current work substantiates the multifunctional role of lignins—synergistic H_2O_2 formation, H_2O oxidation to O_2, no necessity for artificial electron donors, and $OH^{\bullet}$-scavenging activity—in a cascade process combining lignin photocatalysis and UPO biocatalysis. Currently, lignin has been received as a waste and combusted in refinery processes; however, shining light on lignin renders it productive in solar-to-chemical conversion. The renewable biopolymers absorb visible light to generate H_2O_2 and O_2 through O_2 reduction and H_2O oxidation without requiring artificial electron donors. Furthermore, the enantiospecific oxyfunctionalization of inert C-H bonds—a dream reaction in synthetic chemistry—is realized through the merger of lignin photocatalysts and peroxygenases. Lignin's radical scavenging activities play a role in the protection of UPOs from $OH^{\bullet}$-driven inactivation, conducing to the new benchmark ($TTN_{rAaeUPO}$: 81070, >99% *ee*). Overall, this work establishes lignin as an energy conversion material for producing fuels and chemicals, presenting an example of waste-to-wealth conversion.

Experimental procedures

Chemicals and materials

Hydrogen peroxide were purchased from Junsei Chemical Co., Ltd. (Tokyo, Japan). Potassium phosphate monobasic and potassium phosphate dibasic were bought from Samchun Chemical Co., Ltd. (Seoul, Korea). Lignosulfonic acid sodium salt, lignin (alkali), peroxidase from horseradish, nitrotetrazolium blue chloride, 2,2′-azino-bis(3-ethylbenzothiazoline-6-sulfonic acid) diammonium salt, magnesium sulfate, ethyl acetate, 1-octanol, ethylbenzene, (*R*)-1-phenylethanol, (*S*)-1-phenylethanol, acetophenone, iron(III) chloride hexahydrate, and sodium nitrate were purchased from Sigma-Aldrich (St. Louis, MO, USA). O_2 and N_2 gases (purity: 99.999%) were bought from Special Gas Co. (Daejeon, Korea). We used type 1 ultrapure water (18 MΩ cm) from a Direct-Q® 5 UV ultrapure water purification system (Millipore Corp., USA). A recombinant unspecific peroxygenase from *Agrocybe aegerita* (r*Aae*UPO) was prepared as described previously[8,9].

Lignin characterization

We recorded ultraviolet-visible spectra using a V-650 UV-Vis absorption spectrophotometer (JASCO Inc., Japan). Photoluminescence spectra were obtained using a RF-5301PC spectrofluorophotometer (Shimadzu Inc., Japan). Ultraviolet photoelectron spectra were recorded using a Sigma Probe (Thermo VG Scientific, United Kingdom) with a photon energy of 21.2 eV (He I radiation). To make a sample for the photoelectron spectroscopic analysis, we drop-casted a lignin solution (80 mg mL^{-1}) on a fluorine-doped tin oxide (FTO) glass four times and dried it at ambient condition. We employed a potentiostat/galvanostat (WMPG 1000, WonATech Co., Korea) or impedance analyzer (ZIVE SP1, WonATech Co., Korea) to perform photoelectrochemical analyses of lignin photocatalysts in a three-electrode configuration [a

FTO glass (working electrode, geometrical surface area: 2.52 cm^2), Ag/AgCl electrode (reference electrode, 3 M NaCl), and a stainless steel (counter electrode)]. An electrolyte solution was a potassium phosphate buffer (KPi, 100 mM, pH 7.0) containing 1 mg mL^{-1} lignosulfonate or kraft lignin. A solar-simulated light source was a xenon lamp (Newport Co., USA) equipped with an infrared water filter and 400 nm cut-on optical filter.

Lignin-sensitized formation of H_2O_2

The amount of H_2O_2 formed by lignin photocatalysts was determined spectrophotometrically using 2,2'-azino-bis(3-ethylbenzothiazoline-6-sulfonic acid) (ABTS) assay. We dissolved lignin in a KPi buffer (100 mM, pH 7.0, 2.0 mL). We used a xenon lamp (equipped with an infrared water filter and 400 nm longpass filter) to irradiate the sample at 298.15 K. The temperature was maintained using a water bath. The reaction sample (0.05 mL) was mixed with a colorimetric reagent solution [2.5 U horseradish peroxidase and 2 mM ABTS in a phosphate solution (0.95 mL, 100 mM, pH 5.0)]. The absorbance of the mixture was monitored at 420 nm using a V-650 UV-Vis absorption spectrophotometer (JASCO Inc., Japan). When we obtained action spectra of lignin photocatalysts, the incident light was monochromated using a 74004 Cornerstone™ 130 1/8 m monochromator (Newport Co., USA).

NBT and TA assays

We used nitroblue tetrazolium (NBT) and terephthalic acid (TA) assays to detect superoxide ions ($O_2^{\bullet-}$) and hydroxyl radicals ($OH^{\bullet}$), respectively.[33] We added 10 μM NBT or 300 μM TA in a lignin-containing reaction solution. This reaction solution was irradiated with solar-simulated visible light from a xenon lamp equipped with a 400 nm cut-off filter (Newport Co.,

USA). After lignin-driven photocatalysis, we monitored a change in the absorbance at 560 nm and fluorescence intensity at 430 nm (λ_{ex} = 315 nm) to detect NBT formazan and 2-hydroxyterephthalic acid (HTA), respectively.

O_2 quantification

To estimate the amount of O_2 produced by lignin photocatalysts, 1 mg mL^{-1} lignin was dissolved in a N_2-purged KPi buffer (100 mM, pH 7.0, 30 mL). Because the reaction solution was placed and sealed in an airtight chamber (volume: 50 mL), we did not purge N_2 gas (purity: 99.999%) during photocatalytic reactions; otherwise, the chamber would have burst because of excess internal pressure. The solution was exposed to visible light (λ > 400 nm) from a xenon lamp (Newport Co., USA) at 298.15 K. The O_2 molecules in the headspace were quantified using an *in situ* gas chromatography (Micro GC fusion, INFICON Inc., USA) equipped with a Molsieve 5A column and a micro thermal conductivity detector.

Photobiocatalytic reaction and analysis

We prepared a reaction sample by dissolving lignin, r*Aae*UPO, and substrate in a KPi solution (100 mM, pH 7.0, 2.0 mL) in an Eppendorf tube (SPL Life Sciences Co., Korea). The tube was immersed in a water bath to maintain a reaction temperature at 298.15 K and irradiated with a xenon lamp (λ > 400 nm) to promote biocatalytic oxyfunctionalization reactions. When we investigated the kinetics of photoenzymatic reactions, O_2 gas (purity: 99.999%) was purged into reaction solutions (before and during the reactions) to make O_2 an excess reactant. However, we did not bubble O_2 gas during long-term reactions because lignin photocatalysts formed H_2O_2 *via* H_2O oxidation reaction. 10 mM substrate was added every 48 h to

compensate for the high volatility of the substrate. After the photoenzymatic reactions, we extracted oxyfunctionalized products using ethyl acetate, dried them over $MgSO_4$, and quantified them using a 7890A gas chromatograph (Agilent Technologies, USA) equipped with a flame ionization detector and a CP-Chirasil-Dex CB column (25 m × 0.32 mm × 0.25 μm). Detailed oven temperature programs are tabulated in **Supplementary Table 1**. The enantiomeric excess (*ee*), turnover frequency (TOF), and total turnover number (TTN) were calculated using the following equations [**equations (6), (7), and (8)**]:

$$ee\ (\%) = \frac{|\text{Moles of an enantiomer} - \text{Moles of the other enantiomer}|}{\text{Total moles of product}} \times 100 \qquad (6)$$

$$\text{TOF}_{\text{r}Aae\text{UPO}}\ (\text{h}^{-1}) = \frac{[\text{Product}]}{[\text{r}Aae\text{UPO}] \times \text{Time}} \qquad (7)$$

$$\text{TTN}_{\text{r}Aae\text{UPO}} = \frac{\text{Maximum [Product] at a given time}}{[\text{r}Aae\text{UPO}]} \qquad (8)$$

Synthesis and characterization of hematite nanostructure

We synthesized a hematite photoanode via solution-based processing and high temperature annealing as reported previously[39]. We rinsed a FTO glass with acetone, isopropyl alcohol, and deionized water. The glass was immersed in a precursor solution (150 mM $FeCl_3 \cdot 6H_2O$ and 1 M $NaNO_3$) and heated in a Lindberg/Blue M muffle furnace (Fisher Scientific Co., USA) at 100 ºC for 6 h. Subsequently, we annealed the electrode at 800 °C for 20 min. The morphology of a hematite material was examined using a S-4800 field-emission microscope (Hitachi High-technologies Co., Japan). The crystallinity of a hematite film was examined using an Ultima IV X-ray diffractometer (Rigaku Co., Japan) at KAIST Analysis center for Research Advancement (KARA). The element identification of a hematite surface was conducted using

an ESCALAB 250Xi X-ray photoelectron spectrometer (Thermo Scientific., USA) at KARA. The light absorption capability of a hematite material was explored using a SolidSpec-3700 UV-VIS-NIR Spectrophotometer (Shimadzu Corp., Japan).

Antioxidant property of lignin materials

We carried out a photoelectrochemical reaction in a three-electrode configuration [working electrode: α-Fe_2O_3 (geometrical surface area: 2.5 cm^2), reference electrode: Ag/AgCl (3 M NaCl), counter electrode: stainless steel]. These three electrodes are immersed in an O_2-purged KPi buffer (100 mM, pH 7.0) containing 0.3 mM TA with/without lignin energy materials (e.g., kraft lignin, lignosulfonate). We conducted controlled potential photoelectrocatalysis at 0 $V_{Ag/AgCl}$ (0.622 V_{RHE}) under solar-simulated visible light ($\lambda > 400$ nm, photon flux: 1.74 μE cm^{-2} s^{-1}) to form hydroxyl radicals. Note that the lignin was also irradiated with the visible light. After catalytic reactions, we measured the fluorescence intensity of the electrolyte solution at 430 nm ($\lambda_{ex} = 315$ nm) to detect HTA.

Conflicts of interest

The authors declare no competing interests.

Acknowledgements

This work was supported by the National Research Foundation (NRF) *via* the Creative Research Initiative Center (grant no. NRF-2015R1A3A2066191) and the Global Ph.D. Fellowship Program (grant no. NRF-2019H1A2A1075810), Republic of Korea. The authors

would like to thank Gihun Jung from Prof. Byungha Shin's group (Korea Advanced Institute of Science and Technology) for permitting to use an *in situ* gas chromatograph.

Author contributions

J.K. and C.B.P. conceived and designed the research. C.B.P. supervised the research. J.K. performed the experimental works and analyzed the results. F.H. provided biocatalysts. All authors co-wrote the manuscript.

References

1 Kille, S., Zilly, F. E., Acevedo, J. P. & Reetz, M. T. Regio- and stereoselectivity of P450-catalysed hydroxylation of steroids controlled by laboratory evolution. *Nat. Chem.* **3**, 738-743 (2011).

2 Gumulya, Y. *et al.* Engineering highly functional thermostable proteins using ancestral sequence reconstruction. *Nat. Catal.* **1**, 878-888 (2018).

3 Zhang, W. *et al.* Selective aerobic oxidation reactions using a combination of photocatalytic water oxidation and enzymatic oxyfunctionalizations. *Nat. Catal.* **1**, 55-62 (2018).

4 Zhang, W. *et al.* Selective Activation of C−H Bonds in a Cascade Process Combining Photochemistry and Biocatalysis. *Angew. Chem. Int. Ed.* **56**, 15451-15455 (2017).

5 Lee, S. H., Choi, D. S., Kuk, S. K. & Park, C. B. Photobiocatalysis: Activating Redox Enzymes by Direct or Indirect Transfer of Photoinduced Electrons. *Angew. Chem. Int. Ed.* **57**, 7958-7985 (2018).

6 Völler, J.-S. Enzymatic H_2O_2 for biocatalysis. *Nat. Catal.* **2**, 375-375 (2019).

7 Willot, S. J. P. *et al.* Expanding the Spectrum of Light-Driven Peroxygenase Reactions. *ACS Catal.* **9**, 890-894 (2019).

8 van Schie, M. M. C. H. *et al.* Cascading g-C_3N_4 and Peroxygenases for Selective Oxyfunctionalization Reactions. *ACS Catal.* **9**, 7409-7417 (2019).

9 Choi, D. S. *et al.* Bias-Free In Situ H_2O_2 Generation in a Photovoltaic-Photoelectrochemical Tandem Cell for Biocatalytic Oxyfunctionalization. *ACS Catal.* **9**, 10562-10566 (2019).

10 Kim, J. *et al.* Nicotinamide adenine dinucleotide as a photocatalyst. *Sci. Adv.* **5**, eaax0501 (2019).

11 Choi, D. S., Kim, J., Hollmann, F. & Park, C. B. Solar-Assisted eBiorefinery: Photoelectrochemical Pairing of Oxyfunctionalization and Hydrogenation Reactions. *Angew. Chem. Int. Ed.*, doi:10.1002/anie.202006893 (2020).

12 Kim, J. *et al.* Robust FeOOH/BiVO4/Cu(In, Ga)Se_2 tandem structure for solar-powered biocatalytic CO_2 reduction. *J. Mater. Chem. A* **8**, 8496-8502 (2020).

13 Kuk, S. K. *et al.* CO_2-Reductive, Copper Oxide-Based Photobiocathode for Z-Scheme Semi-Artificial Leaf Structure. *ChemSusChem* **13**, 2940-2944 (2020).

14 Lee, Y. W. *et al.* Unbiased biocatalytic solar-to-chemical conversion by FeOOH/$BiVO_4$/perovskite tandem structure. *Nat. Commun.* **9**, 4208 (2018).

15 Kim, J. *et al.* Biocatalytic C=C Bond Reduction through Carbon Nanodot-Sensitized Regeneration of NADH Analogues. *Angew. Chem. Int. Ed.* **57**, 13825-13828 (2018).

16 Huang, Z. *et al.* Enhanced photocatalytic alkane production from fatty acid decarboxylation via inhibition of radical oligomerization. *Nat. Catal.* **3**, 170-178 (2020).

17 Creel, E. B. & McCloskey, B. D. Scalable CO_2-to-oxygenate production. *Nat. Catal.* **1**, 6-7 (2018).

18 Hisatomi, T. & Domen, K. Reaction systems for solar hydrogen production via water splitting with particulate semiconductor photocatalysts. *Nat. Catal.* **2**, 387-399 (2019).

19 Lin, L. *et al.* Molecular-level insights on the reactive facet of carbon nitride single crystals photocatalysing overall water splitting. *Nat. Catal.* **3**, 649-655 (2020).

20 Ulmer, U. *et al.* Fundamentals and applications of photocatalytic CO_2 methanation. *Nat. Commun.* **10**, 3169 (2019).

21 Wang, D., Lee, S. H., Kim, J. & Park, C. B. "Waste to Wealth": Lignin as a Renewable Building Block for Energy Harvesting/Storage and Environmental Remediation. *ChemSusChem* **13**, 2807-2827 (2020).

22 Chen, C.-C., Dai, L., Ma, L. & Guo, R.-T. Enzymatic degradation of plant biomass and synthetic polymers. *Nat. Rev. Chem.* **4**, 114-126 (2020).

23 Wang, M. & Wang, F. Catalytic Scissoring of Lignin into Aryl Monomers. *Adv. Mater.* **31**, 1901866 (2019).

24 Li, C., Zhao, X., Wang, A., Huber, G. W. & Zhang, T. Catalytic Transformation of Lignin for the Production of Chemicals and Fuels. *Chem. Rev.* **115**, 11559-11624 (2015).

25 Sanderson, K. Lignocellulose: A chewy problem. *Nature* **474**, S12-S14 (2011).

26 Wang, D. *et al.* Lignin-fueled photoelectrochemical platform for light-driven redox biotransformation. *Green Chem.* **22**, 5151-5160 (2020).

27 Romero, N. A. & Nicewicz, D. A. Organic Photoredox Catalysis. *Chem. Rev.* **116**, 10075-10166 (2016).

28 Zhang, G., Lan, Z.-A. & Wang, X. Conjugated Polymers: Catalysts for Photocatalytic Hydrogen Evolution. *Angew. Chem. Int. Ed.* **55**, 15712-15727 (2016).

29 Boehm, A. M., Wieser, J., Butrouna, K. & Graham, K. R. A new photon source for ultraviolet photoelectron spectroscopy of organic and other damage-prone materials. *Org. Electron.* **41**, 9-16 (2017).

30 Koppenol, W. H., Stanbury, D. M. & Bounds, P. L. Electrode potentials of partially reduced oxygen species, from dioxygen to water. *Free Radical Biol. Med.* **49**, 317-322 (2010).

31 Sadeghifar, H. & Ragauskas, A. Lignin as a UV Light Blocker—A Review. *Polymers* **12**, 1134 (2020).

32 Hou, H., Zeng, X. & Zhang, X. Production of Hydrogen Peroxide by Photocatalytic Processes. *Angew. Chem. Int. Ed.*, doi:10.1002/anie.201911609 (2020).

33 Yoon, J. *et al.* Piezobiocatalysis: Ultrasound-Driven Enzymatic Oxyfunctionalization of C–H Bonds. *ACS Catal.* **10**, 5236-5242 (2020).

34 Schultz, D. M. & Yoon, T. P. Solar Synthesis: Prospects in Visible Light Photocatalysis. *Science* **343**, 1239176 (2014).

35 Choi, D. S. *et al.* Photoelectroenzymatic Oxyfunctionalization on Flavin-Hybridized Carbon Nanotube Electrode Platform. *ACS Catal.* **7**, 1563-1567 (2017).

36 Zhao, J., Nanjo, T., de Lucca, E. C. & White, M. C. Chemoselective methylene oxidation in aromatic molecules. *Nat. Chem.* **11**, 213-221 (2019).

37 Simon, T. *et al.* Redox shuttle mechanism enhances photocatalytic H_2 generation on Ni-decorated CdS nanorods. *Nat. Mater.* **13**, 1013-1018 (2014).

38 Huang, C. *et al.* Unveiling the Structural Properties of Lignin–Carbohydrate Complexes in Bamboo Residues and Its Functionality as Antioxidants and Immunostimulants. *ACS Sustainable Chem. Eng.* **6**, 12522-12531 (2018).

39 Kim, K., Lee, B. I., Chung, Y. J., Choi, W. S. & Park, C. B. Hematite-Based Photoelectrode Materials for Photoelectrocatalytic Inhibition of Alzheimer's β-Amyloid Self-Assembly. *Adv. Healthc. Mater.* **6**, 1601133 (2017).

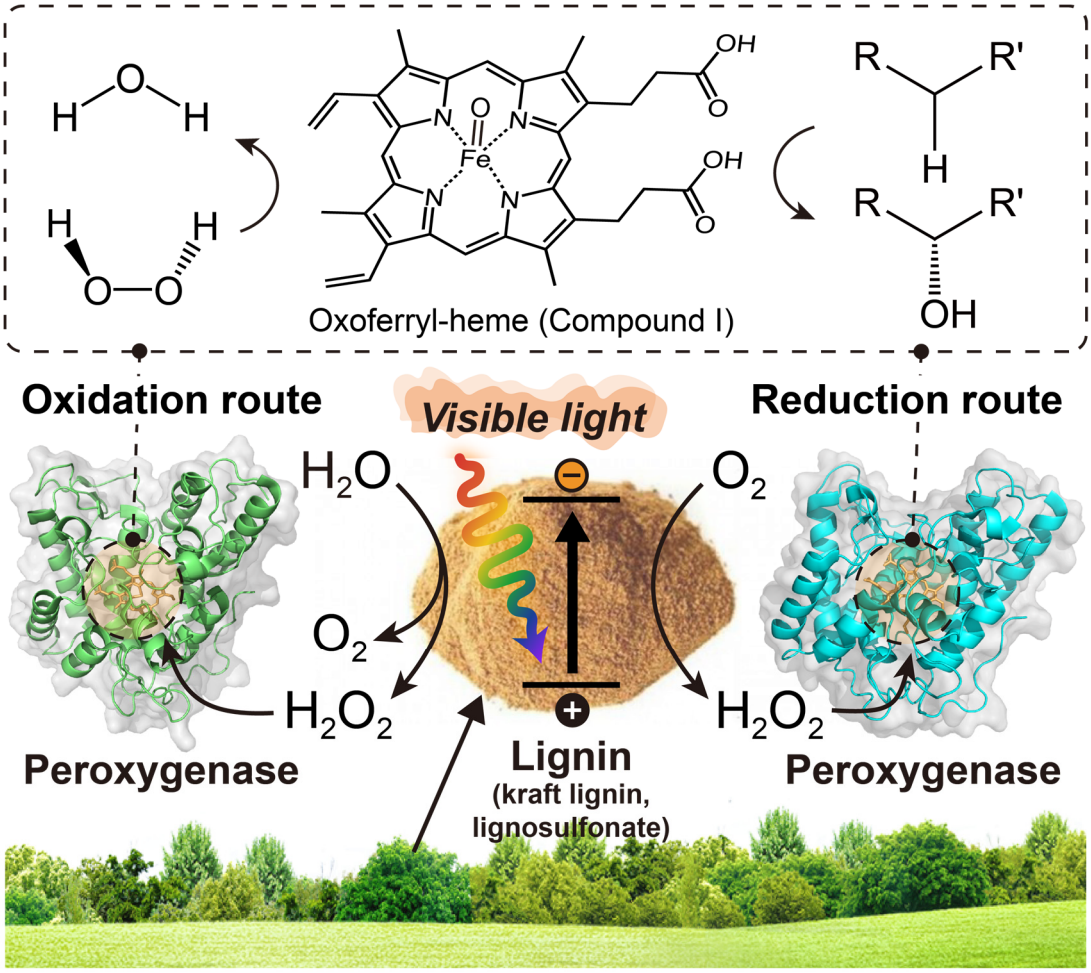

Fig. 1: Illustration of a photoenzymatic oxyfunctionalization reaction through the synergetic integration of lignin photocatalysts and peroxygenase redox biocatalysts. Photoactivation of lignin energy materials (e.g., lignosulfonate and kraft lignin) under visible light drives redox reactions, such as (i) reduction of O_2 to H_2O_2 and (ii) oxidation of H_2O to H_2O_2 and O_2. The *in situ* generated H_2O_2 activates oxoferryl-heme (Compound I, redox center) of peroxygenases to catalyze stereoselective oxyfunctionalization reactions (e.g., hydroxylation and epoxidation).

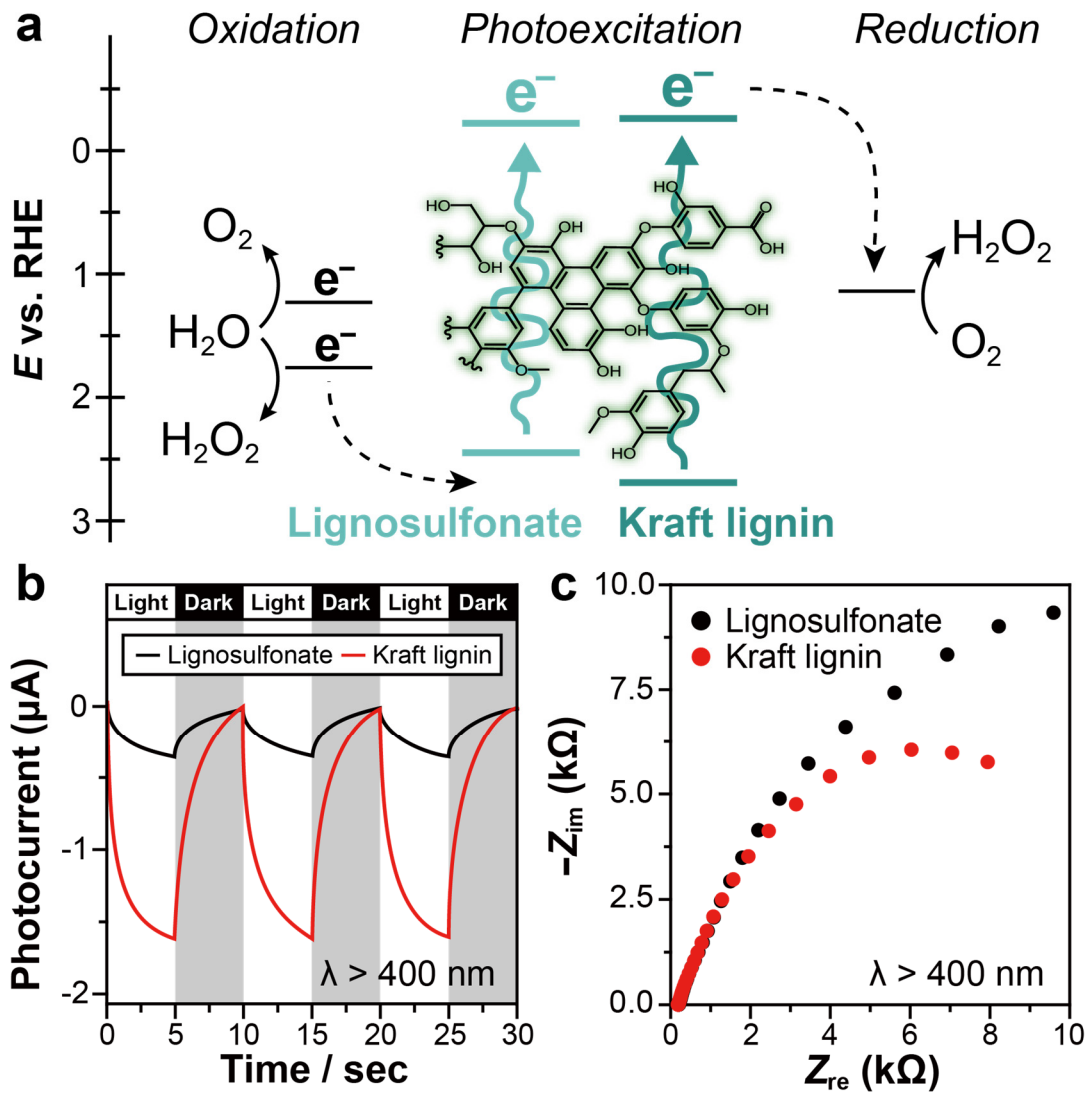

Fig. 2: Electronic and photophysical properties of lignin photocatalysts. (**a**) Energy diagram for lignin-sensitized O_2 reduction to H_2O_2 and H_2O oxidation to H_2O_2 and O_2. (**b**) Transient photocurrent response of lignin photocatalysts at −0.028 V_{RHE} under solar-simulated visible light. (**c**) Electrochemical impedance spectroscopic analysis in the form of Nyquist plots under visible light at −0.028 V_{RHE}. Z_{re} and Z_{im} indicate real and imaginary impedance, respectively. Light source: xenon lamp (λ > 400 nm, photon flux: 0.58 μE cm^{-2} s^{-1}).

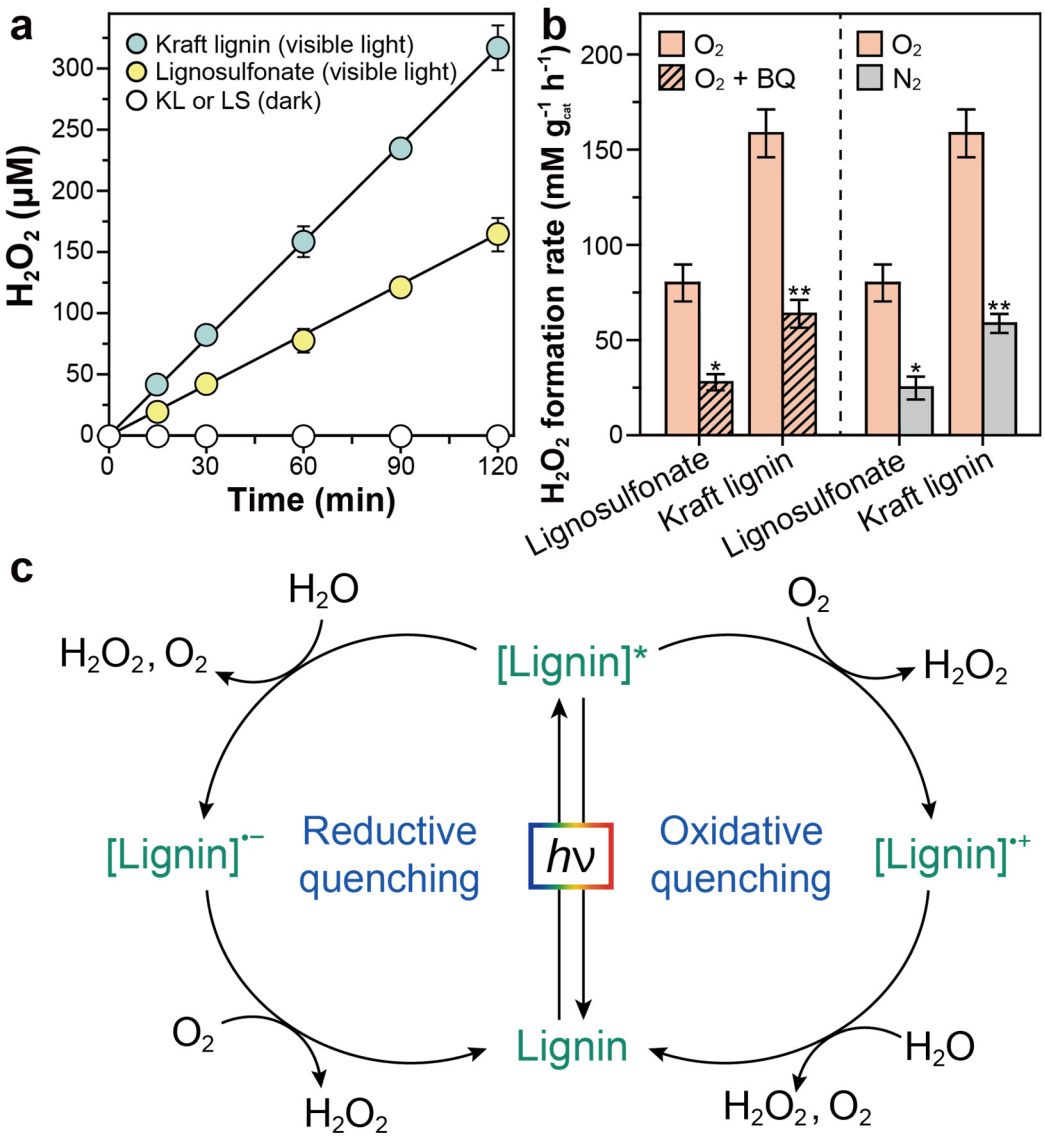

Fig. 3: Lignin-sensitized production of H_2O_2 under visible light and its mechanism study. (**a**) Visible light-driven generation of H_2O_2 by lignin photocatalysts. Reaction conditions: 1 mg mL^{-1} lignin photocatalyst in an O_2-enriched KPi buffer (100 mM, pH 7.0) under dark or light conditions (λ > 400 nm, photon flux: 0.58 μE cm^{-2} s^{-1}) at 298.15 K. (**b**) Effect of 1,4-benzoquinone (left panel) or N_2 (right panel) on lignin-sensitized H_2O_2 production. Reaction conditions: 1 mg mL^{-1} lignin photocatalyst and 1 mM *p*-benzoquinone in a KPi solution (100 mM, pH 7.0) at 298.15 K. Error bars correspond to the standard deviation (n = 3). Single and double asterisks (* and **) denote two groups, the difference of which was statistically insignificant. (**c**) Two possible photocatalytic pathways of lignin-sensitized formation of H_2O_2 and O_2.

Table 1: Substrate scope of photobiocatalytic oxyfunctionalization reaction using lignin photocatalysts and r*Aae*UPO biocatalysts.

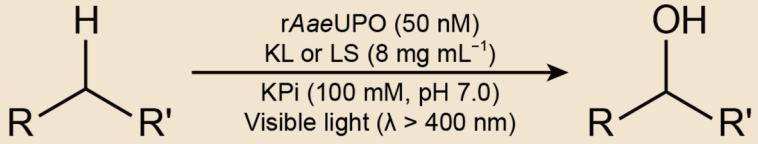

Entry[a]	Product	Concentration (mM)		*ee* (%)		$TTN_{rAaeUPO}$	
		KL	LS	KL	LS	KL	LS
1	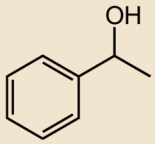	3.63	4.05	>99 (*R*)	>99 (*R*)	72552	81070
2	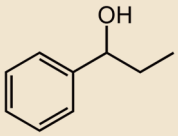	1.46	1.72	>99 (*R*)	>99 (*R*)	29181	34439
3	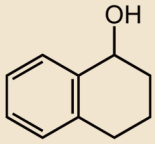	2.77	3.00	>99 (*R*)	>99 (*R*)	55361	60051
4	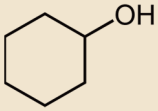	1.73	1.86	NA	NA	34644	37264
5	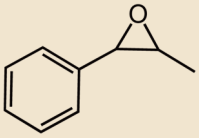	1.26	1.35	>99 (1*R*, 2*S*)	>99 (1*R*, 2*S*)	25282	27064

[a]Reaction condition: 8 mg mL^{-1} lignin photocatalyst, 50 nM r*Aae*UPO, and 10 mM substrate in a KPi buffer (100 mM, pH 7.0, O_2 purged) under visible light (λ > 400 nm, photon flux: 1.74 μE cm^{-2} s^{-1}) at 298.15 K. NA: not applicable.

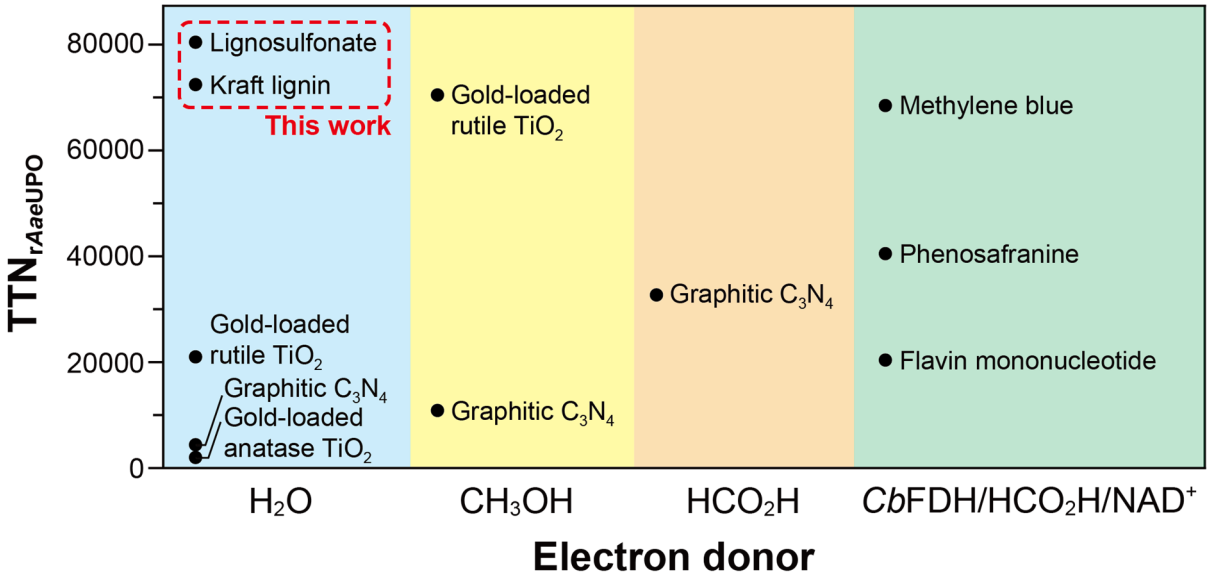

Fig. 4: Comparison of total turnover numbers of state-of-the-art photoenzymatic systems that use r*Aae*UPO catalysts and visible light for ethylbenzene hydroxylation. References: gold-loaded rutile TiO_2 nanoparticle[3,4], gold-loaded anatase TiO_2 nanoparticle[3], graphitic carbon nitride[8], methylene blue[7], phenosafranine[7], and flavin mononucleotide[7]. *Cb*FDH: formate dehydrogenase from *Candida boidinii*.